Turkish Journal of Electrical Engineering & Computer Sciences
http://journals.tubitak.gov.tr/elektrik/
Research Article

Turk J Elec Eng & Comp Sci
(2018) 26: 1180 – 1189

doi:10.3906/elk-1706-101

Circularly polarized implantable antenna characterization for retinal prosthesis systems

Ademola Oluwaseun KAKA[1], **Mehmet TOYCAN**[1,*], **Stuart Douglas WALKER**[2]
[1]Department of Electric and Electronic Engineering, Faculty of Engineering, Cyprus International University, Nicosia, Northern Cyprus
[2]School of Computer Science and Electronic Engineering, University of Essex, Colchester, UK

Received: 08.06.2017 • **Accepted/Published Online:** 22.12.2017 • **Final Version:** 30.05.2018

Abstract: We describe a miniaturized antenna design for retinal prosthesis applications that enhances data transfer between the implant and external camera. The circularly polarized and conformal 2.4–2.48 GHz microstrip patch antenna was simulated inside the vitreous humor and is intended for biomedical applications. Modified Hilbert and serpentine geometries were used for the proposed implant antenna design. Capacitive radiator loading offered miniaturized dimensions of 5.8 × 6.5 × 2 mm^3 (width × height × thickness mm^3). A truncated design enhanced the intrinsic circular polarization characteristics to >3 dB axial ratio. Polydimethylsiloxane substrate and superstrate materials were used to achieve an S_{11} value below –15 dB across the frequency range with biocompatible characteristics. The simulated peak gains for left-hand circular polarization and right-hand circular polarization at 2.45 GHz were –50 dBi and –60 dBi, respectively. These relatively small values were due to the high conductivity of the vitreous humor (σ = 1.53 S/m), which imposed significant losses. Overall, the proposed antenna had an omnidirectional radiation pattern and +8.45 dBm input to meet the specific absorption rate regulation limit.

Key words: Implant antenna, miniaturized, circular polarization, retinal prosthesis systems

1. Introduction

Implant antennas concerned with wireless telemetry monitoring of health conditions continue to attract interest [1]. One example is age-related macular degeneration (AMD), a genetic syndrome that causes loss of central vision [2]. This results in reading and face recognition difficulties. Late-stage forms of the disease even cause blindness among elderly individuals [3]. AMD is estimated to increase by 50% in 2020. Retinitis pigmentosa (RP) is another group of hereditary diseases of the eye that can also lead to eventual blindness. In 2013, the Committee for Orphan Medicinal Products noted that RP affected fewer than 3.7 in 10,000 people in the European Union. Although this is equivalent to 188,000 people, no satisfactory methods are authorized in the European Union for treating RP [4]. For instance, approximately 20,000 people have been diagnosed with RP, also known as night blindness, in Turkey [5].

A retinal prosthesis system (RPS) to mitigate the effects of AMD and RP diseases is therefore worth investigation. The Argus II project is a well-known RPS that provides electrical stimulation of the retina to induce visual perception in blind individuals [6]. The block diagram of the system is illustrated in Figure 1, which appears courtesy of Prof Dr Mark S Humayun and Second Sight Medical Products.

*Correspondence: mtoycan@ciu.edu.tr

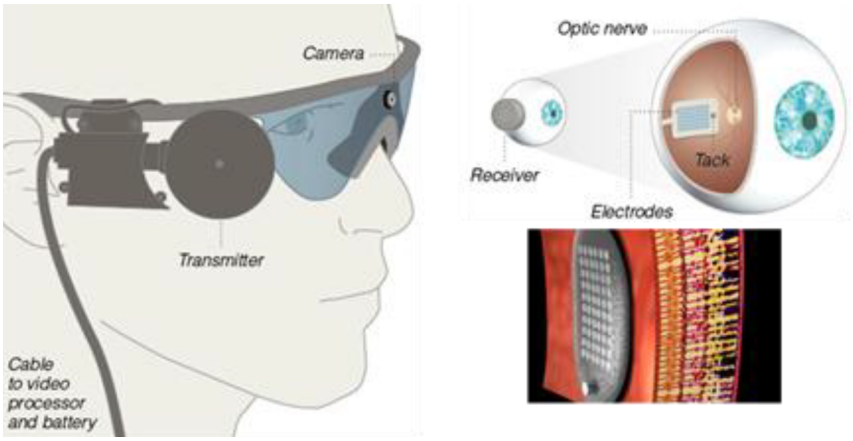

Figure 1. Argus II RPS (http://www.2-sight.eu/ee/).

As shown in Figure 1, a miniaturized external video camera is placed on the spectacles to capture images. Then the recorded video is transmitted to a small on-body computer. The video is processed here according to predetermined transformation instructions and sent back to the spectacles via a cable. After that, the processed signals are transmitted to an implant antenna in a wireless medium placed in the RPS inside the eye. These received signals are transferred to the electrode array, which emits small pulses of electricity. These pulses stimulate the retina's healthy cells while avoiding the damaged photoreceptors. This could enhance the transmission of visual information along the optic nerve to the brain in order to create the perception of patterns of light [6]. The Argus II retinal prosthesis system is marked for "European Conformity" (Conformité Européene – CE) and has been available in the European Economic Area since 2011. In addition, the system is accepted as a humanitarian device with authorization by the Food and Drug Administration of the United States [6]. The Argus II RPS has been implanted in patients from various countries who have totally lost their central vision [5,6].

Here, we focus solely on the design and characterization of an intraocular antenna. Compared to well-known antenna design techniques, implantable antennas have some unique challenges in antenna miniaturization, impedance matching, bandwidth, multiband operation low-power requirements (specific absorption rate (SAR) limitation), and biocompatibility [7]. These features must be optimized in order to achieve acceptable performance, considering that the detuning effects inside the human body may have a considerable impact on the antenna response. Previous studies have shown that both antenna gain and efficiency decrease due to the high dielectric loss of the human body [8]. The medical implant communications service (MICS) band (402– 405 MHz) and the industrial, scientific, and medical (ISM) bands (915, 2450, and 5800 MHz) are usually preferred for wireless health monitoring systems [8,9]. Consequently, many simulations and experiments have investigated tissue-equivalent liquids [7], mimicking gels [10], and animals [11].

2. Design methodology

The flowchart of the simulated antenna design methodology is depicted in Figure 2. The first objective (Step 1) was to initialize the antenna design parameters for the human eyeball model (vitreous humor as the surrounding material) with a diameter of 24 mm and check for the return loss (S_{11}) values. Hilbert fractal geometry and serpentine radiator geometry are applied and modified as design parameters with capacitive loading techniques

in order to achieve the desired resonance characteristics, with optimal S_{11} results, for the ISM bandwidth (2.4–2.48 GHz). Human tissues, including vitreous liquid, are conductive and could short-circuit the antenna during direct contact with the metal part of the implant. Design parameters for Hilbert fractal and serpentine radiator geometries are modified to achieve this. The second objective (Step 2) was to achieve CP with reduced multipath and improved bit error rate characteristics. In order to achieve CP, the four edges of the radiating patch are removed as design modifications. PDMS substrate and superstrate material ($\varepsilon_r = 2.68$; $\tan\,\delta = 0.04$) are considered to achieve biocompatible and conformal characteristics [24]. The third objective (Step 3) was to consider and study different dielectric substrates as design modifications to understand their effect on implant antenna performance. Then a superstrate dielectric layer is introduced to achieve biocompatibility. It has been a challenging research objective to insulate the antenna implant with a thin layer of low-loss biocompatible coating. There are some well-known materials that could be used for this approach, such as Teflon ($\varepsilon_r = 2.1$; $\tan\,\delta = 0.001$), MACOR ($\varepsilon_r = 6.1$; $\tan\,\delta = 0.005$), ceramic alumina ($\varepsilon_r = 9.4$; $\tan\,\delta = 0.006$), polyether ether ketone (PEEK) ($\varepsilon_r = 3.2$; $\tan\,\delta = 0.0076$), and zirconia ($\varepsilon_r = 29$; $\tan\,\delta = 0.001$) [1]. As a final objective (Step 4), the thickness of the superstrate was optimized as a design parameter, since its value enhances the ease of inserting an implant inside human tissue and has a significant impact for decreasing power loss.

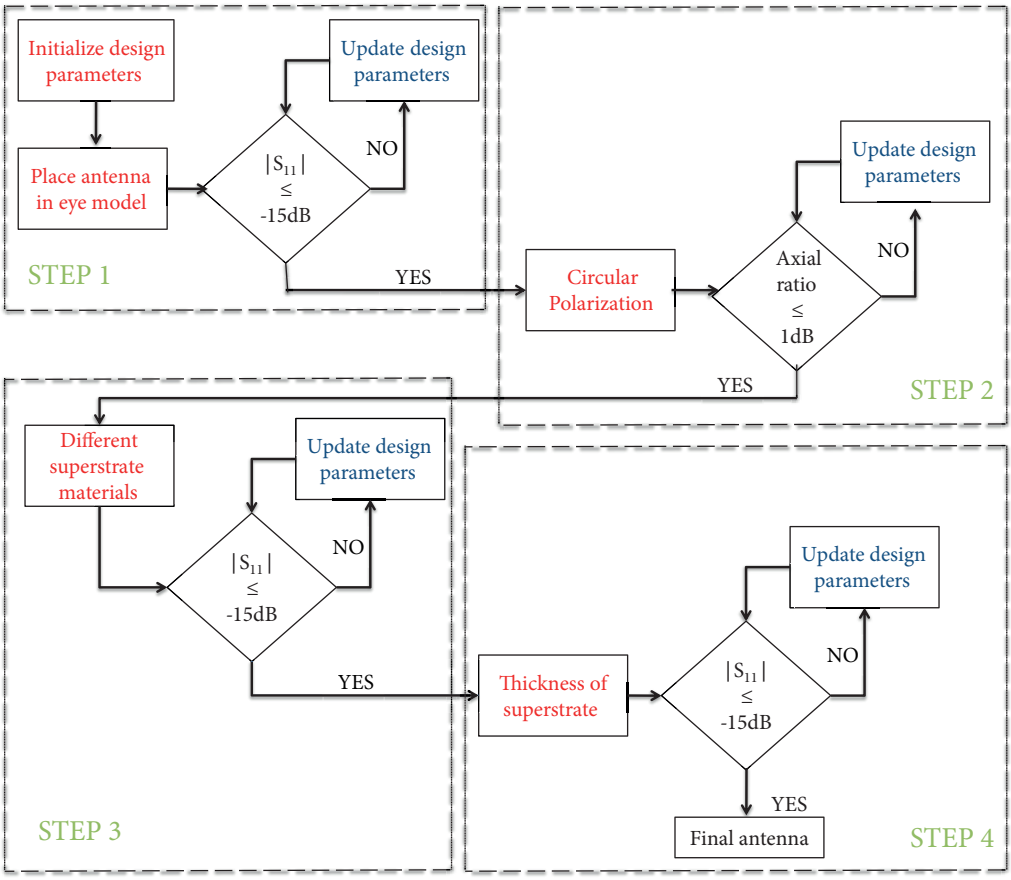

Figure 2. Proposed generic four-step methodology for implantable antenna design.

3. Proposed antenna geometry parameterization

The proposed implant antenna consists of three layers: layer 1 is a ground plane and layer 2 is radiating elements. Finally, layer 3 is a superstrate plane to achieve biocompatibility. The first, second, and final step modifications of the proposed patch geometry are shown in Figures 3a–3c, respectively. It was designed on a PDMS substrate with ε_r of 2.68 and tan δ of 0.04. The position of the feed is centered on the xy-axis. Two major design guidelines, Hilbert fractal geometry and serpentine geometry, were applied to achieve the proposed antenna's radiating element geometry. The initial shape was a square since it is easy to modify and is centrosymmetric on (0, 0). A first modification was to insert the Hilbert fractal geometry that was applied to the (–2.9, –2.75) and (2.9, 2.75) regions. The Hilbert generation process has been considered in previous research [23] and was spread through 2/3 of the lateral edges and connected. Finally, the long strips were removed to enhance longer electrical length, as seen in Figure 3a. As the second modification, serpentine geometry (slits) were applied and slits were removed just under the top edges of Hilbert geometries on the patch in order to increase the capacitive nature of the design, as depicted in Figure 3b. For the final modification, the proposed antenna geometry was truncated, as shown in Figure 3c, in order to achieve a CP antenna with approximately zero AR value. Sections protruded from the four corners of the radiating patch with the same dimensions of $dx \times dy$ to split the fundamental resonant TM_{11} mode into two near-degenerate orthogonal modes with equal amplitudes and 90° phase difference. Therefore, the electrical length had to be increased while maintaining the spatial dimension. The increased capacitive loading was also used to reduce the AR as much as possible, to <3 dB. In addition, the antenna does not have any sharp edges that could cause any harm to the human eye. Final antenna geometry parametrization is summarized in Table 1. With the applied capacitive loading, patch size was reduced with a fixed operation frequency of 2.4 GHz. Slots from x_a to x_i are optimized to lower the resonant frequency while increasing the length of current path. The truncated section parameter Y is 1.8 mm and it is the maximum removal that can be achieved for the proposed antenna.

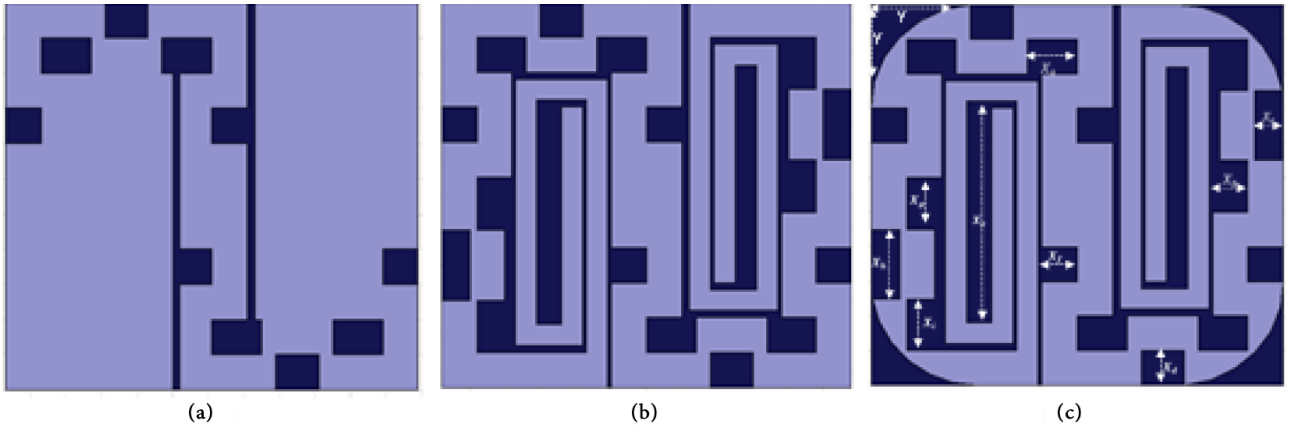

Figure 3. (a) First design modifications, (b) second design modifications, and (c) final truncated antenna design.

Table 1. Final antenna geometry parametrization.

x_a	x_b	x_c	x_d	x_e	x_f	x_g	x_h	x_i
0.7 mm	0.5 mm	0.4 mm	0.5 mm	3.2 mm	0.51 mm	0.75 mm	1 mm	0.75 mm

An extra layer of PDMS was used on top of the patch antenna as shown in Figure 4a. The PDMS superstrate and the PDMS substrate together enhance the conformal structure with an improvement in the

antenna performance and biocompatible characteristics. Noting again that human tissues are conductive and could short-circuit the antenna during direct contact with the implant, this extra layer results in a 0.5 mm thicker design.

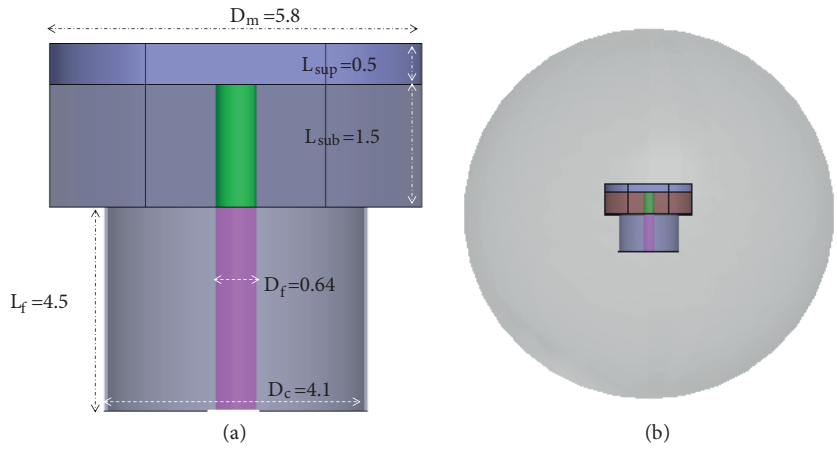

Figure 4. Top view of each layer and (b) proposed antenna inside the eyeball model simulation. All the units are in mm.

The antenna was developed as an implant, so it should evaluated in an environment that is similar to the human eye. Therefore, the proposed implant antenna was placed inside vitreous humor liquid, as shown in Figure 4b. The vitreous humor sphere is modeled on the size of the human eyeball, which has a radius of 12.5 mm, and the antenna is embedded at the center of the sphere. It has high dielectric constant and conductivity characteristics at 2.4 GHz (?$_r$ = 68.21, σ = 1.53 S/m, and tan δ = 0.27) [13]. The superstrate material PDMS performs better due to the lower conductivity of the PDMS relative to the higher conductivity of vitreous humor. A probe feed application is considered due to its simplicity for future measurement techniques. All design parameters, including the location of the probe feed, were carefully adjusted for 50 Ω impedance matching.

4. Simulation results

Finite element methods were used to analyze the proposed antenna with commercially available full-wave 3D Ansoft HFSS software, with the design consideration set to the boundary considerations of the human biological system. First, a radiating patch was simulated on PDMS substrate with a thickness of 1.5 mm, ε_r of 2.68, and tan δ of 0.04. Low-permittivity dielectric substrate was considered for the proposed implantable patch antennas to achieve better conductivity due to the higher permittivity of vitreous humor, resulting in lower resonant frequencies with good transmission characteristics. PDMS superstrate was also used as a superstrate material for the proposed implant design.

Figure 5a depicts the simulation analysis of the effects of the first, second, and final design modifications, as seen in Figure 3, on the antenna performance by monitoring simulated S_{11} variations over the ISM bandwidth (2.4–2.48 GHz). In addition, different antenna modifications' effects on CP property performance were also simulated, as illustrated in Figure 5b. As seen in Figure 5a, the second design modification has the best ($S_{11} \leq -20$ dB) results over the ISM bandwidth. This was expected, since the serpentine radiator leads to a further increment of the electrical length of the antenna, which raises the input resistance of the antenna. This modification also gives the surface current a larger path, which also increases the input resistance for the

antenna on the proposed bandwidth range. With the truncated design, return loss is decreased to –14 dB, since the current path is decreased with the removal of edges. According to Figure 5b, the truncated design yields the lowest AR values (better than 2 dB) by removing the edges, as seen in Figure 3c. This would lead to near-degenerate orthogonal modes with equal amplitudes and 90° phase difference. For higher values of the truncated section parameter Y, better CP transmission characteristics can be achieved, as seen in Figure 5b. Therefore, the maximum value (1.8 mm) was used for all simulation results.

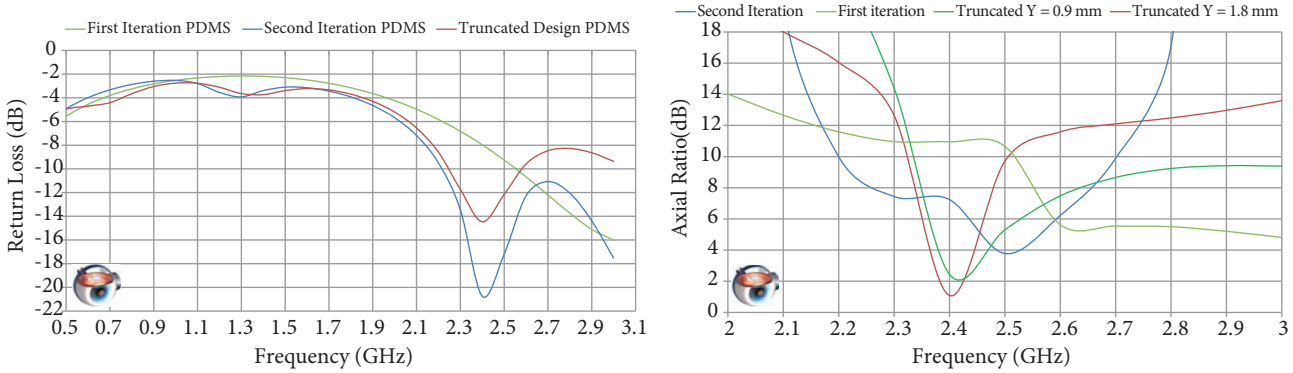

Figure 5. First, second, and final truncated design configurations. (a) Return loss comparison, (b) AR comparison.

In addition to PDMS, a polymer (PEEK), Teflon, and three ceramics (alumina, MACOR, and zirconia) were considered for the proposed implant antenna that is designed for biomedical monitoring systems. Figure 6 depicts a simulation analysis of how different substrate and superstrate materials affect the antenna performance by monitoring simulated S_{11} variations over the ISM bandwidth (2.4–2.48 GHz). The thickness of the proposed combinations is 0.5 mm. As seen in Figure 6, the PDMS superstrate material yields satisfactory results ($S_{11} \leq -10$ dB) over the ISM bandwidth (2.4–2.48 GHz). This is an expected characteristic, since materials with higher permittivity result in lower resonant frequency because the effective wavelength is shorter. For instance, the proposed antenna operates between 1.9 and 2.2 GHz with the zirconia superstrate ($\varepsilon_r = 29$) and between 2.3 and 3 GHz with the Teflon superstrate. The proposed antenna operating frequency ranges and performances with different superstrate materials are summarized in Table 2. In accordance, the PDMS superstrate material is used for all simulation analysis. It was shown in [12] that increments in superstrate thickness would result in better S_{11} characteristics. Figure 7 depicts the simulation analysis for the proposed antenna with different superstrate thicknesses over the ISM bandwidth in order to achieve acceptable AR values. On the other hand, the eyeball has a typical diameter of 24 mm and space limitation is an important aspect for this reason. In addition, it was also realized from [21] that thinner superstrate materials would have fewer frequency shifts. It can be seen from Figure 7 that for a thickness of 0.5 mm, the AR bandwidth covers from 2.4 to 2.48 GHz for AR of <3 dB. Therefore, a superstrate thickness of 0.5 mm was considered for the rest of the simulation analysis and good polarization purity was achieved. The voltage standing wave ratio of the proposed antenna over the ISM bandwidth was less than 1.5. These results prove good matching characteristics and correlate with the return loss measurements.

The plot of real and imaginary parts of the input impedance versus frequency of the proposed antenna for the ISM band is depicted in Figure 8. The imaginary part is close to zero (approximately 2) and the real part is approximately 50 Ω. It can be stated that the antenna is fairly well matched to 50 Ω and has stable characteristics. Simulated two-dimensional radiation and gain patterns of the proposed antenna in vitreous

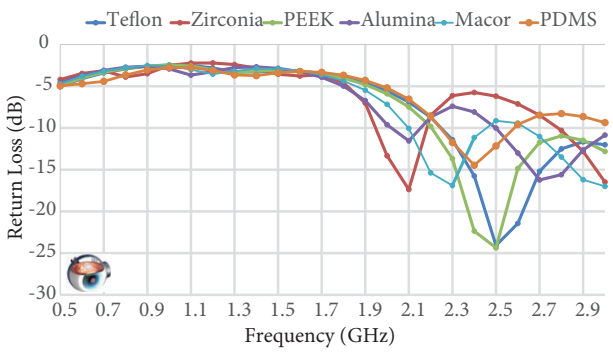

Figure 6. Return loss analysis with different superstrate materials.

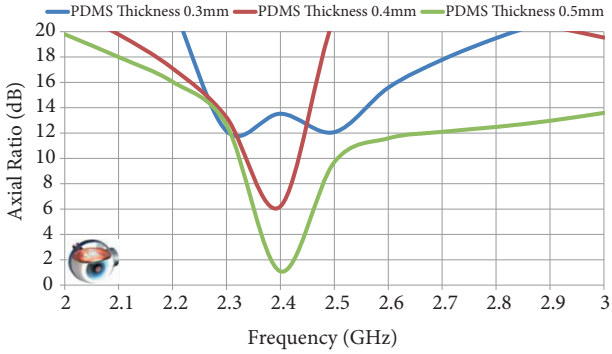

Figure 7. Performances of the proposed antenna with different PDMS thicknesses.

Table 2. Different superstrate materials' operating bandwidth ranges.

Superstrate materials	Teflon	PDMS	PEEK	MACOR	Alumina	Zirconia
Permittivity (ε_r)	2.1	2.68	3.2	6.1	9.4	29
Bandwidth (GHz): $S_{11} \leq -10$ dB	2.3–3	2.3–2.5	2.2–3	2.1–2.45	2–2.17	1.9–2.2

humor at 2.4 GHz are depicted in Figures 9a and 9b, respectively, for both left-hand circular polarization (LHCP) and right-hand circular polarization (RHCP). As seen in Figure 9a, the simulated peak gains for LHCP and RHCP at 2.45 GHz are –50 dBi and –60 dBi, respectively. It can be stated that the main polarization of this proposed antenna is LHCP. The implant antenna gain is negative because the antenna is embedded into vitreous humor, which has high conductivity ($\sigma = 1.53$ S/m). The surrounding tissue model introduces high dissipation, which causes losses on the propagating signals. Eq. (1) defines the relationship between the attenuation constant, relative permittivity, and conductivity [25].

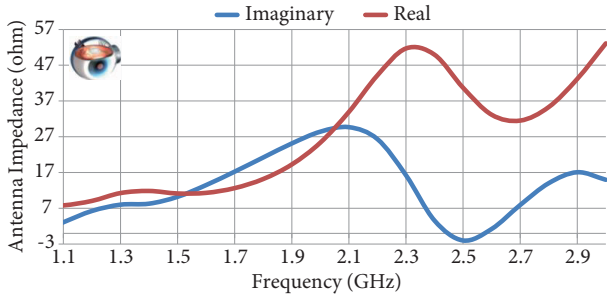

Figure 8. Input impedance: real part – imaginary part of the proposed implantable antenna.

$$\alpha = \omega \sqrt{\frac{\mu\varepsilon}{2}\left[1 + \frac{\sigma}{\varepsilon\omega} - 1\right]} \tag{1}$$

Here, α is the attenuation constant (Np/m), μ is permeability (H/m), ε is permittivity (F/m), and σ is conductivity (S/m). It could be stated from Eq. (1) that a higher dielectric constant and/or higher conductivity would result in higher attenuation constant, which explains the lower gain characteristics when the vitreous humor was implemented. It was shown in previous studies that the superstrate layer is advantageous in terms of

antenna gain [20]. It can be observed from Figure 9b that the antenna can give omnidirectional characteristics for both LHCP and RHCP with stable radiation patterns. Therefore, transmission does not require accurate orientation alignment. The SAR values were produced under a 1 W input power condition. Therefore, to adhere to the SAR regulation limit of 1.6 W/kg, the incident power should not exceed 7 mW. The electromagnetic energy profile is illustrated in Figure 10.

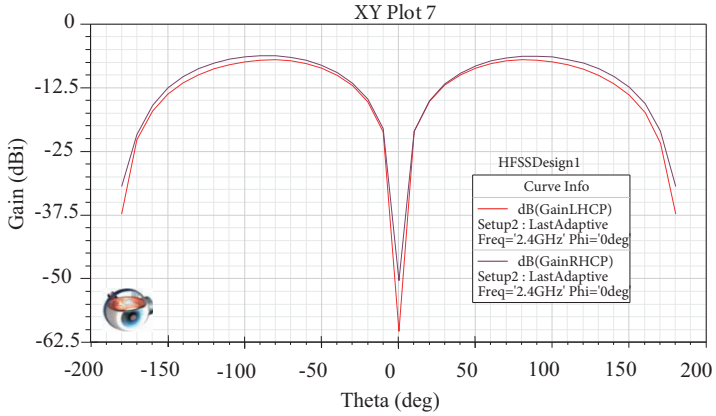

(a)

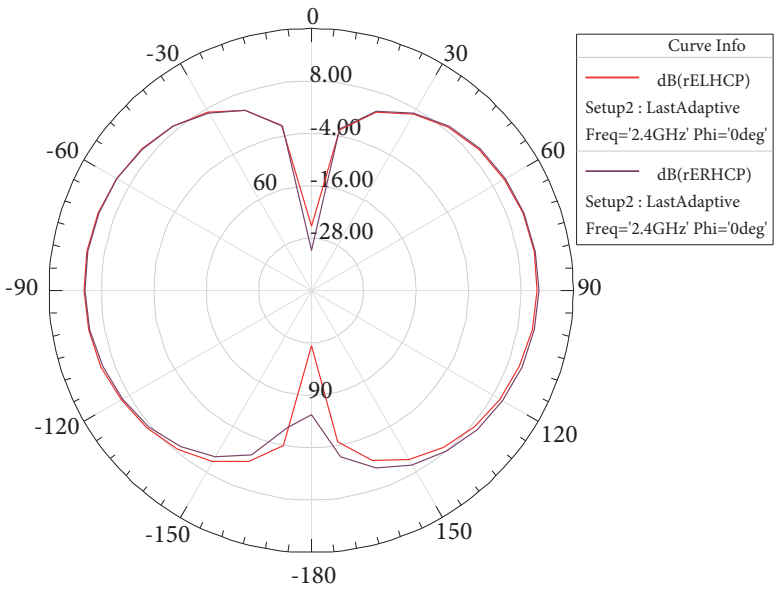

(b)

Figure 9. Two-dimensional (a) gain pattern and (b) radiation pattern of the proposed antenna at 2.4 GHz, LHCP (red line) and RHCP (purple line).

5. Conclusion

This paper presents a miniaturized implantable CP microstrip patch antenna created using modified Hilbert and serpentine geometries for retinal prosthesis systems. The result is an ISM band (2.4–2.48 GHz) implantable antenna. Core fractal properties of the Hilbert curve, such as space-filling and self-similarity, ensure miniaturized

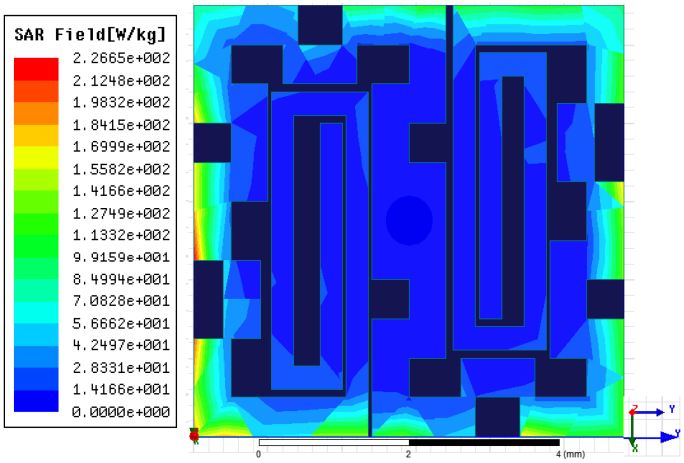

Figure 10. Proposed antenna showing the electromagnetic energy (SAR profile) at 2.45 GHz.

5.8 × 6.5 × 2 mm^3 (width × height × thickness mm^3) characteristics. Based on this research, several simulations were performed. First, the proposed antenna was simulated inside vitreous humor liquid. In addition to the modified fractal geometries, a capacitive loading technique was applied to the radiating patch to achieve better impedance matching and better performance characteristics on the desired resonance frequencies. Second, the truncated design was utilized by removing the edges of the patch to realize a CP implantable patch antenna with an AR better than 3 dB. Third, various superstrate materials were considered and simulated to achieve biocompatibility. It was realized that materials with higher permittivity result in lower resonant frequency because the effective wavelength is shorter. In accordance, PDMS substrate and superstrate materials were used for the antenna design in order achieve operation in the desired frequency range and conformity with better antenna characteristics (S_{11} below –15 dB) over the ISM bandwidth. Finally, superstrate thickness was considered and it was realized that an increment in superstrate thickness would result in better S_{11} characteristics. However, a thickness of 0.5 mm was applied, since the implant would be embedded inside the eye for retinal prosthesis systems. A coaxial probe was used as a feeding line for the further experimental analysis. Stable and omnidirectional performance was obtained for the radiation patterns over the full-band ISM bandwidth. The simulated peak gains for LHCP and RHCP at 2.45 GHz were –50 dBi and –60 dBi, respectively. The implant antenna yielded small gain values due to the high conductivity characteristic of the vitreous humor (σ = 1.53 S/m), which causes losses in the propagating signals. In addition, the SAR distribution patterns were presented and it was realized that the incident power should not exceed 7 mW. The proposed implant antenna shows promising simulation results in vitreous humor and can be used for retinal prosthesis systems.

References

[1] Kiourti A, Nikita KS. A review of implantable patch antennas for biomedical telemetry: challenges and solutions. IEEE Antenn Propag M 2012; 54: 210-228.

[2] Lim LS, Mitchell P, Seddon JM, Holz FG, Wong TY. Age-related macular degeneration. Lancet 2012; 379: 1728-1738.

[3] Augustin AJ. Optical coherence tomography imaging and quantitative assessment for monitoring dry age-related macular degeneration. European Ophthalmic Review 2012; 6: 1-8.

[4] European Medicines Agency. EU/3/13/1146: Public Summary of Opinion on Orphan Designation: Unoprostone Isopropyl for the Treatment of Retinitis Pigmentosa. Brussels, Belgium: European Medicines Agency, 2015.

[5] Özmert E, Demirel S. Endoscope-assisted and controlled Argus II epiretinal prosthesis implantation in late-stage retinitis pigmentosa: a report of 2 cases. Case Rep Ophthalmol 2016; 7: 315-324.

[6] Rachitskaya AV, Yuan A. Argus II retinal prosthesis system: an update. Ophthalmic Genet 2016; 37: 260-266.

[7] Soontornpipit P, Furse CM, Chung YC. Design of implantable microstrip antenna for communication with medical implants. IEEE T Microw Theory 2004; 52.8: 1944-1951.

[8] Kaka AO, Toycan M, Walker SD. Miniaturized stacked implant antenna design at ISM band with biocompatible characteristics. International Journal for Computation and Mathematics in Electrical and Electronic Engineering 2015; 34: 1270-1285.

[9] Medical Implant Communication Service. Federal Register. Rules and Regulations 1999. Washington, DC, USA: MICS, 1999.

[10] Karacolak T, Hood AZ, Topsakal E. Design of a dual-band implantable antenna and development of skin mimicking gels for continuous glucose monitoring. IEEE T Microw Theory 2008; 56: 1001-1008.

[11] Karacolak T, Cooper R, Butler J, Fisher S, Topsakal E. In vivo verification of implantable antennas using rats as model animals. IEEE Antenn Wirel Propag Let 2010; 9: 334-337.

[12] Permana H, Fang Q, Rowe WST. Hermetic implantable antenna inside vitreous humor simulating fluid. Prog Electromagn Res 2013; 133: 571-590.

[13] Gosalia K, Humayun MS, Lazzi G. Impedance matching and implementation of planar space-filling dipoles as intraocular implanted antennas in a retinal prosthesis. IEEE T Antenn Propag 2005; 53: 2365-2373.

[14] Izdebski PM, Rajagopalan H, Rahmat-Samii Y. Conformal ingestible capsule antenna: a novel chandelier meandered design. IEEE T Antenn Propag 2009; 57: 900-909.

[15] Toh BY, Cahill R, Fusco VF. Understanding and measuring circular polarization. IEEE T Educ 2003; 46: 313-318.

[16] Nasimuddin, Qing X, Chen ZN. Compact asymmetric-slit microstrip antennas for circular polarization. IEEE T Antenn Propag 2011; 59: 285-288.

[17] Liu C, Xiao S, Guo YX, Bai YY, Tang MC, Wang BZ. Compact circularly-polarized microstrip antenna with symmetric-slit. Electron Lett 2012; 48: 195-196.

18 Bao XL, Ammann MJ. Dual-frequency circularly-polarized patch antenna with compact size and small frequency ratio. IEEE T Antenn Propag 2007; 55: 2104-2107.

[18] Dong Y, Toyao H, Itoh T. Compact circularly-polarized patch antenna loaded with metamaterial structures. IEEE T Antenn Propag 2012; 59: 4329-4333.

[19] Oh J, Sarabandi K. Low profile, miniaturized, inductively coupled capacitively loaded monopole antenna. IEEE T Antenn Propag 2012; 60: 1206-1213.

[20] Liu C, Guo YX, Xiao S. Capacitively loaded circularly polarized implantable patch antenna for ISM band biomedical applications. IEEE T Antenn Propag 2014; 62: 2407-2417.

[21] Gabriel S, Lau RW, Gabriel C. The dielectric properties of biological tissues: II. Measurements in the frequency range 10 Hz to 20 GHz. Phys Med Biol 1996; 41: 2251-2269.

[22] Kaka AO, Toycan M, Bashiry V, Walker SD. Modified Hilbert fractal geometry, multi-service, miniaturized patch antenna for UWB wireless communication. International Journal for Computation and Mathematics in Electrical and Electronic Engineering 2012; 6: 1835-1849.

[23] Tiercelin N, Coquet P, Sauleau R, Senez V, Fujita H. Polydimethylsiloxane membranes for millimeter-wave planar ultra-flexible antennas. J Micromech Microeng 2006; 16: 2389-2395.

[24] Ulaby FT. Fundamentals of Applied Electromagnetics. Upper Saddle River, NJ, USA: Pearson Education, 2007.